

# Simulated identification of epidemic threshold in finite-size networks

Panpan Shu,<sup>1</sup> Wei Wang,<sup>1</sup> and Ming Tang<sup>1,2,\*</sup>

<sup>1</sup>Web Sciences Center, University of Electronic Science and Technology of China, Chengdu 610054, China

<sup>2</sup>State key Laboratory of Networking and Switching Technology,  
Beijing University of Posts and Telecommunications, Beijing 100876, China

(Dated: December 7, 2024)

Epidemic threshold is one of the most important features of the epidemic dynamics. Based on a lot of numerical simulations of classic Susceptible-Infected-Recovered (SIR) and Susceptible-Infected-Susceptible (SIS) models on various types of networks, we study the simulated thresholds for finite-size networks. We confirm that the susceptibility measure goes awry for the SIR model due to the bimodal distribution of outbreak sizes near the critical point, while the simulated thresholds of the SIS and SIR models can be accurately determined by analyzing the peak of the epidemic variability. We further verify the accuracy of theoretical predictions of the heterogeneous mean-field theory (HMF) and of the quenched mean-field theory (QMF), by comparing them with the simulated threshold of the SIR model obtained from the variability measure. The results show that the HMF prediction agrees very well with the simulated threshold, except the case that the networks are disassortive, in which the QMF prediction is more close to the simulated threshold.

PACS numbers:

## I. INTRODUCTION

Models for disease propagation are the foundation of the study of spreading dynamics on complex networks [1, 2]. Two epidemic models of particular importance are the susceptible-infected-susceptible (SIS) and susceptible-infectious-recovered (SIR) models [3]. At each time step, an infected node can infect each of its susceptible neighbors with probability  $\lambda$ . At the same time, the infected nodes become susceptible again in the SIS model or recover in the SIR model with probability  $\mu$ . In the SIS model, a critical value of the effective transmission rate  $\lambda/\mu$  separates the absorbing phase with only healthy nodes from the active phase with a stationary density of infected nodes. Differently, no steady state is allowed in the SIR model, but a threshold still exists above which the final fraction of infected nodes is finite [4].

The traditional theoretical study on the epidemic threshold of the SIS model was based on the heterogeneous mean-field (HMF) theory, which means that all the nodes within a given degree are considered to be statistically equivalent [5, 6]. According to the HMF theory, the epidemic threshold of SIS model is given by [7, 8]

$$\lambda_c^{\text{HMF}} = \frac{\langle k \rangle}{\langle k^2 \rangle}, \quad (1)$$

where  $\langle k \rangle$  and  $\langle k^2 \rangle$  are the first and second moments of degree distribution  $P(k)$  [9], respectively. On networks with power-law scaling  $P(k) \sim k^{-\gamma}$  [9, 10], where  $\gamma$  is the degree exponent, one obtains a vanishing threshold in the thermodynamic limit for  $\gamma \leq 3$ , while the threshold is finite for  $\gamma > 3$  [11]. As the quenched structure of the network and dynamical correlations between the state of adjacent nodes are neglected in the HMF theory [12], researchers proposed

an important improvement over the HMF theory—quenched mean-field (QMF) theory. The QMF theory fully preserves the actual quenched structure of the network described as its adjacency matrix, and the epidemic threshold is predicted to be [13–15]

$$\lambda_c^{\text{QMF}} = \frac{1}{\Lambda_N}, \quad (2)$$

where  $\Lambda_N$  is the maximum eigenvalue of the adjacency matrix of a given network. Given the scaling of  $\Lambda_N$  with the maximum degree,  $\Lambda_N \sim \{\sqrt{k_{\max}}, \langle k^2 \rangle / \langle k \rangle\}$  [16], the epidemic threshold predicted by the HMF theory is the same as that from the QMF theory for  $\gamma < 5/2$ , while for  $\gamma > 5/2$  the QMF prediction vanishes in the thermodynamic limit [28]. Moreover, for a network with large size  $N$ , the more accurate SIS threshold

$$\lambda_c^{(2)} = \lambda_c^{\text{QMF}} + o\left(\frac{\lambda_c^{\text{QMF}}}{N}\right) \quad (3)$$

is estimated by the second-order mean-field approximation [17].

The earliest theoretical study on the SIR model is under the assumption of homogeneous mixing, showing that the SIR threshold is inversely proportional to the average connectivity  $\langle k \rangle$  [3]. At the HMF level [18], the threshold of the SIR model takes the value

$$\lambda_c = \frac{\langle k \rangle}{\langle k^2 \rangle - \langle k \rangle}. \quad (4)$$

For the SIR model can be mapped to the bond percolation model, Eq. (4) coincides with the critical point of bond percolation [19]. According to the QMF theory, the SIR threshold is Eq. (2). Eqs. (2) and (4) are the same for random networks without degree-degree correlations.

As the existing theories have inherent defects, (e.g., the HMF theory neglects the quenched structure of the network, dynamical correlations are ignored in QMF theory) [20], some

\*Electronic address: tangminghuang521@hotmail.com

numerical methods have been proposed to check the accuracy of the different theoretical estimations. Three conventional methods are finite-size scaling [21], susceptibility [22], and lifetime [23]. Generally, the finite-size scaling method allows the precise numerical determination of the critical point in absorbing-state phase transitions (e.g., contact process, Ising model), but it can not estimate the transition point accurately if big corrections to scaling are present on networks with strong heterogeneity [24, 25]. So far the susceptibility method and lifetime method are only applied to the SIS model [23, 26]. Different from the case in the SIS model, the outbreaks change from an infinitesimal fraction ( $\lambda < \lambda_c$ ) to a finite fraction ( $\lambda \geq \lambda_c$ ) [27]. The widely accepted method for estimating the SIR threshold should be the percolation theory [19], according to which the outbreak size is finite above the critical point. However, the critical value of the finite outbreak size can not be measured quantitatively in numerical simulations. Although the HMF theory has been indicated to be more accurate for predicting the SIR threshold in configuration model [28], the systematic investigation of the accurate determination of the SIR threshold is still lacking.

In this work, we perform a lot of numerical simulations of the SIR model on networks with finite size, and present a simulated method by analyzing the peak of the epidemic variability [29, 30] to determine the epidemic threshold. The accuracy of this method is checked by applying it on random regular networks (RRN), where the HMF is exact. The method is also employed to study the cases of scale-free networks and real networks.

We organize this paper as follows. In Sec. II, we describe the epidemic dynamics and present simulated method for determining epidemic threshold. In Sec. III, we investigate some critical properties of the SIS and SIR dynamics, and discuss the validity of the numerical methods. In Sec. IV, the simulated thresholds of the SIR model on scale-free (SF) networks and real networks are discussed. Sec. V gives conclusions.

## II. SIMULATED IDENTIFICATION OF EPIDEMIC THRESHOLD

In simulations, we consider the SIS and SIR models for epidemics in discrete time. At the beginning, half of nodes are randomly chosen as seeds in the SIS model. As the number of initial infected nodes affect the final outbreak size, we assume that only one node is infected at the initial time in the SIR model. The simulations are implemented as follows: at each time step, each susceptible node  $i$  becomes infected with probability  $1 - (1 - \lambda)^{N_i}$  if it contacts with one or more infected neighbors, where  $N_i$  is the number of its infected neighbors. At the same time, all infected nodes are cured and become again susceptible at rate  $\mu$  in the SIS model, while they recover (or die) at rate  $\mu$  and the recovered nodes acquire immunity in the SIR model. Time is incremented by  $\Delta t = 1$ , and the SIS or SIR process is iterated with parallel updating. The SIS process ends after a long time step, and the SIR process ends when there are no more infected nodes. Without lack of generality, we set  $\mu = 1$ .

For a RRN with constant degree  $k$ , the HMF predictions for the SIS and SIR thresholds are accurate, namely  $\lambda_c^{SIS} = 1/k$  and  $\lambda_c^{SIR} = 1/(k - 1)$  [5], respectively. By comparing with the HMF predictions on RRNs, Figs. 1 (a) and (b) check the accuracy of simulated threshold  $\lambda_p^\chi$  from the susceptibility

$$\chi = N \frac{\langle \rho^2 \rangle - \langle \rho \rangle^2}{\langle \rho \rangle}, \quad (5)$$

where  $\rho$  denotes the prevalence  $\rho_I$  (i.e., the steady density of infected nodes in the SIS model) or the outbreak size  $\rho_R$  (i.e., the final density of removed nodes in the SIR model). We find the SIS threshold determined by the susceptibility  $\chi$  is close to  $\lambda_c^{SIS} = 1/k$ , but the simulated threshold of the SIR model is larger than  $\lambda_c^{SIR} = 1/(k - 1)$ . In other words, the susceptibility  $\chi$  becomes invalid for estimating the threshold of the SIR model.

Here we predict the epidemic threshold by the variability [29, 30], defined as

$$\Delta = \frac{\sqrt{\langle \rho^2 \rangle - \langle \rho \rangle^2}}{\langle \rho \rangle}, \quad (6)$$

which can be explained as the standard deviation of the epidemic prevalence (outbreak size), and is a standard quantity to determine critical point in equilibrium phase on magnetic system [24]. The insets of Figs. 1 (a) and (b) show that the variability  $\Delta$  reaches a maximum at the critical point, so we estimate the epidemic threshold from the position of the peak of the variability  $\lambda_p^\Delta$ . For the SIS model, we compare  $\lambda_p^\Delta$  with the HMF prediction  $1/k$  and pair approximation  $1/(k - 1)$  [31] respectively. We find  $\lambda_p^\Delta$  is consistent with the HMF prediction, and is smaller than the pair approximation for small  $k$ . With the increase of  $k$ , the gap between them decreases as  $1/k \simeq 1/(k - 1)$ . For the SIR model,  $\lambda_p^\Delta$  is also consistent with the HMF prediction  $\lambda_c^{SIR} = 1/(k - 1)$ . To make a further comparison with Ref. [26], we consider the relationship between the epidemic threshold and network size in Figs. 1 (b) and (d). Once the degree  $k$  is given, the simulated thresholds  $\lambda_p^\chi$  and  $\lambda_p^\Delta$  do not change with  $N$ . Our synchronous updating accounts for the difference between  $\lambda_c^{SIS} = 1/k$  in this work and  $\lambda_c^{SIS} = 1/(k - 1)$  in Ref. [26]. Now, a new problem has arisen: why the variability  $\Delta$  performs well but the susceptibility  $\chi$  goes awry for the SIR model?

## III. ANALYSIS OF THE EPIDEMIC PREVALENCE NEAR THE CRITICAL POINT

To deal with that problem illuminated in Sec. II, we investigate the distribution of  $\rho_I$  ( $\rho_R$ ) in the SIS (SIR) model, and the fluctuation of epidemic prevalence (outbreak size)  $\zeta = \langle \rho^2 \rangle - \langle \rho \rangle^2$ . Fig. 2 shows these results for a RRN with  $k = 10$ . We find that the distribution of the prevalence near the SIS threshold is very different from the outbreak size distribution near the SIR threshold.

For the SIS model, we obtain the simulated threshold  $\lambda_c = 1/\langle k \rangle \simeq 0.1$ . Below the threshold (i.e.,  $\lambda < \lambda_c$ ), a nonzero  $\rho_I$

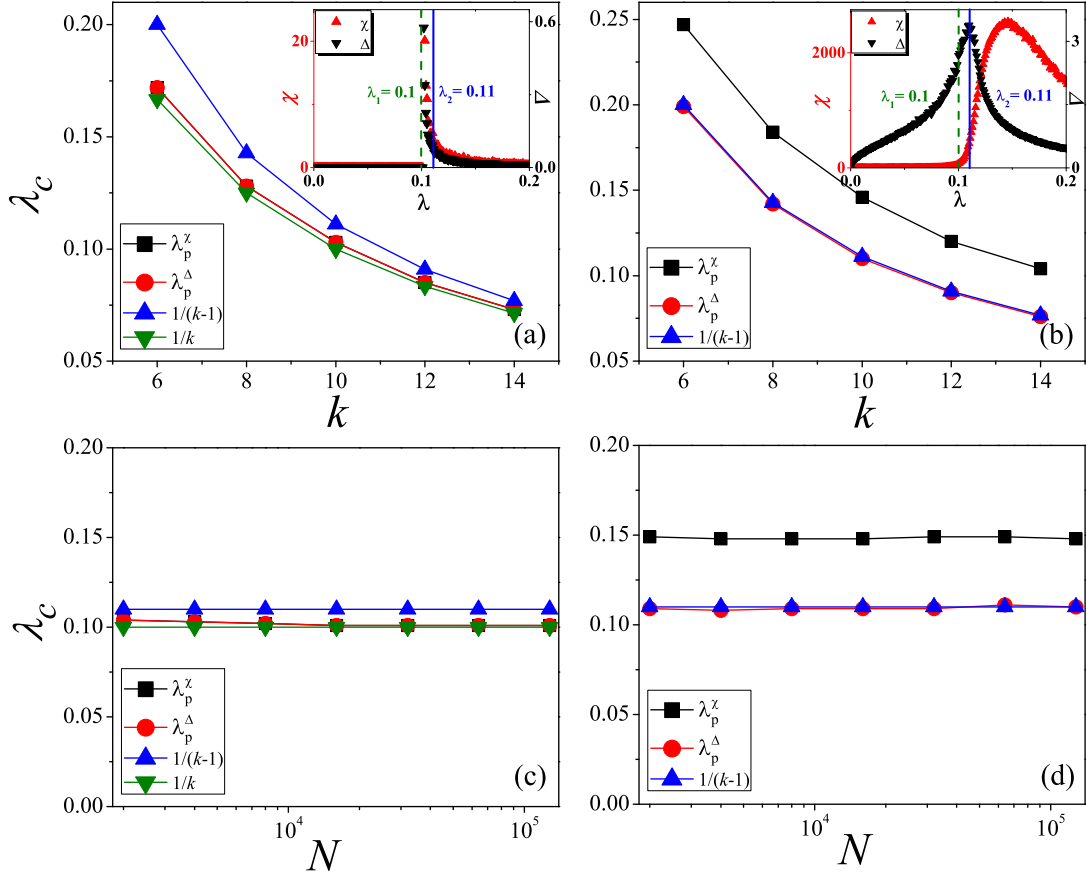


FIG. 1: (Color online) Comparison of theoretical thresholds with simulated thresholds on RRs. The threshold  $\lambda_c$  vs. degree  $k$  for SIS (a) and SIR (b), where  $N$  is set at  $10^4$ . The threshold  $\lambda_c$  vs. network size  $N$  for SIS (c) and SIR (d), where  $k$  is set at 10. In each subfigure, “squares”, “circles”, “triangleups”, and “triangledowns” denote  $\lambda_p^x$ ,  $\lambda_p^\Delta$ ,  $1/(k-1)$  and  $1/k$ , respectively.

can hardly exist, since the disease will eventually die out. At the threshold (i.e.,  $\lambda = 0.1$ ), although the prevalence is close to be an exponential distribution, the probability of  $\rho_I = 0$  is maximum, which means the prevalence is still very small. Above the threshold (e.g.,  $\lambda=0.105$  and  $0.11$ ), the prevalence approximates a normal distribution, where the position of the peak value is determined by the average density of infected nodes  $\langle \rho_I \rangle$ . Fig. 2 (c) shows that the fluctuation of  $\rho_I$  in SIS model is on the order of one-thousandth of the fluctuation of  $\rho_R$  in SIR model. When  $\lambda < \lambda_c$ ,  $\zeta$  is zero, and the corresponding susceptibility  $\chi$  and variability  $\Delta$  are zero. When  $\lambda \geq \lambda_c$ ,  $\zeta$  is finite and changes little with  $\lambda$ , while  $\langle \rho_I \rangle$  increases with  $\lambda$ . As a result, the peaks of the susceptibility  $\chi$  and the variability  $\Delta$  appear simultaneously at  $\lambda \simeq \lambda_c$  [see the inset of Fig. 1 (a)].

For the SIR model, the variability  $\Delta$  determines the simulated threshold  $\lambda_c = 1/(\langle k \rangle - 1) \simeq 0.11$ . In Fig. 2 (b), the outbreak sizes follow approximately an exponential distribution at  $\lambda = 0.1$ . Near the critical point  $\lambda \simeq \lambda_c$ , the outbreak sizes follow a power-law distribution  $P(\rho_R) \sim \rho_R^\alpha$  with a cutoff at some value, where  $\alpha \simeq -1.5$  [32–34]. Since the disease maybe die out quickly or infect a subset of nodes when  $\lambda > \lambda_c$ , the distribution of outbreak sizes is bimodal [35, 36],

with two peaks occurring at  $\rho_R = 1/N$  and  $\rho_R \simeq 0.2$  at  $\lambda = 0.12$ , respectively. Therefore, the fluctuation of the outbreak sizes increases monotonically with  $\lambda$  near the critical point in Fig. 2 (c).

Moreover, the theoretical distribution of the small epidemic size (see Appendix) is compared with the results obtained by numerical simulations in Fig. 2 (b). The theoretical probability from Eq. (10) is consistent with the simulated results for relatively small outbreak size ( $\rho_R < 0.05$ ). Near the critical point, the theoretical results prove that the outbreak sizes indeed obey a power-law distribution with the exponent -1.5. When  $\lambda > \lambda_c$ , some large outbreak sizes constitute a lump in the simulated scattergram, but the probability of large outbreak sizes can not be solved from Eq. (10). We thus speculate that the non-ignorable lump may be influential in numerically determining the SIR threshold.

To verify the rationality of the speculation, Fig. 3 investigates the effectiveness of the variability and susceptibility measures under some cutoff hypothesis. We set the cutoff value of the outbreak size as  $r_c$ , which means the maximum outbreak size is  $r_c$  in Fig. 2 (b). Three kinds of  $r_c$  are considered, where  $r_c = 0.05$  corresponds to the maximum small outbreak size before the lump appears in the simulated dis-

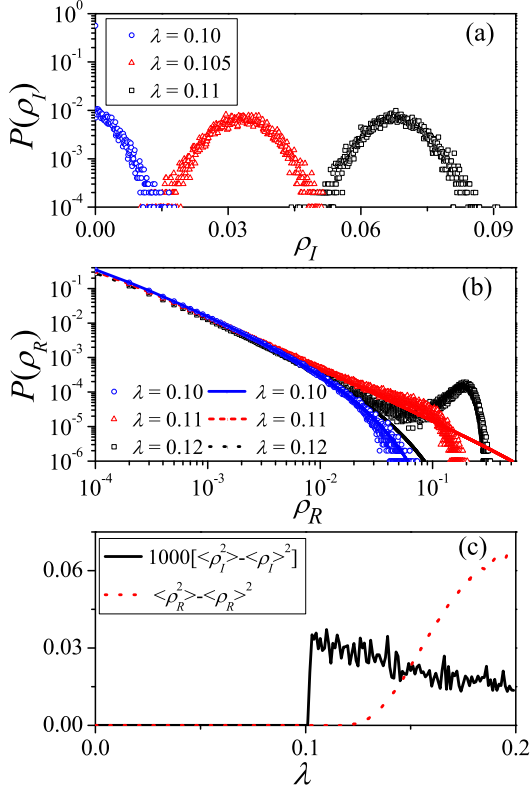


FIG. 2: (Color online) Critical distribution and fluctuations on a RRN. (a) Simulated distribution of the prevalence  $\rho_I$  in SIS model for  $\lambda = 0.10$  (circles),  $\lambda = 0.105$  (triangles), and  $\lambda = 0.11$  (squares). (b) Simulated distribution of outbreak sizes  $\rho_R$  in SIR model for  $\lambda = 0.10$  (circles),  $\lambda = 0.11$  (triangles), and  $\lambda = 0.12$  (squares), where blue solid, red short dash and black dot lines respectively represent the theoretical distributions given by Eq. (10). (c) Fluctuations of the prevalence  $1000(\langle \rho_I^2 \rangle - \langle \rho_I \rangle^2)$  (solid line) and the outbreak size  $\langle \rho_R^2 \rangle - \langle \rho_R \rangle^2$  (dot line). The parameters are chosen as  $N = 10^4$  and  $k = 10$ .

tribution,  $r_c = 0.1$  means that the distribution consists of a part of the lump, and  $r_c = 0.2$  means that there is a complete lump in the distribution. When calculating the susceptibility in Fig. 3 (a), all possible outbreak sizes are considered when  $\lambda \leq \lambda_c$ , while only the outbreak size with  $\rho_R \leq r_c$  is required at  $\lambda > \lambda_c$ . The susceptibility measure can indeed give a quite accurate estimate of the SIR threshold when the whole lump is ignored (i.e.,  $r_c = 0.05$ ). With the increase of  $r_c$ , the peak of the susceptibility  $\chi$  gradually shifts to the right for large outbreak sizes are considered. This indicates that the existence of the lump leads to the susceptibility  $\chi$  lose its effectiveness on determining the SIR threshold.

We have found from simulations that the cutoff value  $r_c$  does not affect the simulated threshold  $\lambda_p^\Delta$  corresponding to the first peak of  $\Delta$ . Then, the effectiveness of the variability  $\Delta$  is further checked in theory. As the simulated distribution of the large outbreak sizes is concentrated, we assume the probability distribution of the lump is a Dirac delta function in the theory. That is to say, there is a lump located at  $r = r_c$  with  $P(r_c) = 1 - \sum_{\rho_R < r_c} P(\rho_R)$  in the theoretical probability

distribution diagram of the outbreak size. Then, we plot the variability measure as a function of  $\lambda$  for different values of  $r_c$  in Fig. 3 (b). The variability  $\Delta$  measures the heterogeneity of the distribution of outbreak sizes, which is strongest at the critical point. Therefore, the peak of the variability measure does not change with the size of the lump, as shown in Fig 3(b).

From the above analysis, we can conclude that the variability  $\Delta$  is effective in determining the epidemic threshold of SIR model, while the bimodal distribution of outbreak sizes when  $\lambda > \lambda_c$  leads to the obvious difference between the HMF prediction and the simulated threshold from the susceptibility  $\chi$ .

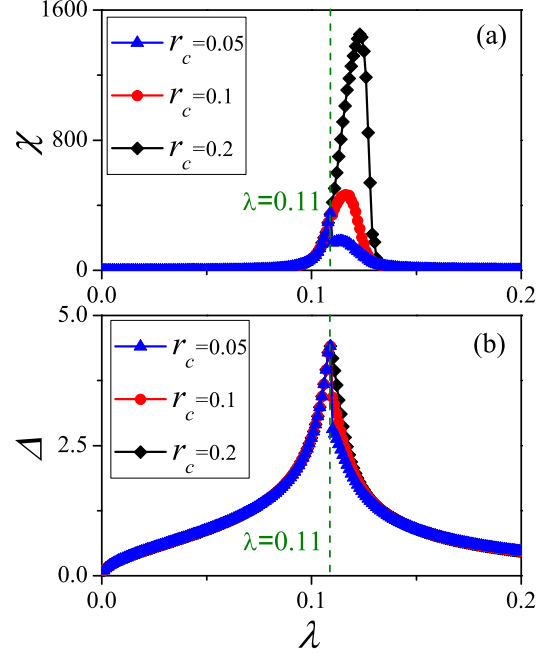


FIG. 3: (Color online) Susceptibility  $\chi$  and variability  $\Delta$  with cutoff as a function of  $\lambda$  on a RRN. (a)  $\chi$  vs.  $\lambda$ , where only the small outbreak sizes with  $\rho_R \leq r_c$  are considered when  $\lambda > \lambda_c$ . (b)  $\Delta$  vs.  $\lambda$ , where the theoretical distribution of the lump is assumed to be a Dirac delta function. ‘triangles’, ‘circles’ and ‘diamonds’ denote cutoff values  $r_c = 0.05, 0.1$  and  $0.2$ , respectively. The parameters are chosen as  $N = 10^4$  and  $k = 10$ .

#### IV. APPLICATIONS

In this section, we focus on discussing the accuracy of the theoretical estimations of the HMF and of the QMF on scale-free and real networks, by comparing them with the simulated threshold from the variability  $\Delta$ .

##### A. Epidemic threshold of scale-free networks

We first build scale-free networks (SFNs) with degree distribution  $P(k) \sim k^{-\gamma}$  based on the configuration model [9].

The so-called structural cutoff  $k_{max} \sim N^{1/2}$  and natural cutoff  $k_{max} \sim N^{1/\gamma-1}$  [37] are considered to constrain the maximum possible degree of the vertices  $k_{max}$  in the networks. We consider the SIR model on SFNs with structural cutoff in Figs. 4 (a) and (c), where the SIR threshold increases monotonically with the degree exponent  $\gamma$  and decreases linearly with the network size  $N$  [22]. Since the structural cutoff makes the degree-degree correlations vanish [37], the HMF prediction  $\lambda_c^{HMF}$  is much close to the simulated threshold  $\lambda_p^\Delta$ , while there is an obvious difference between the QMF prediction  $\lambda_c^{QMF}$  and  $\lambda_p^\Delta$ . According to Ref. [38], the epidemic threshold is related to the largest degree  $k_{max}$ , whose variation with  $N$  depends strongly on  $\gamma$ . Thus,  $\lambda_c$  drops rapidly for  $\gamma = 2.25$  and changes slowly with  $N$  for  $\gamma = 3.5$  [see Fig. 4 (c)].

The SIR thresholds on SFNs with natural cutoff are considered in Figs. 4 (b) and (d), where the variation of SIR threshold with  $\gamma$  and  $N$  are similar to the result on SFNs with natural cutoff. The HMF prediction is still accurate but there is a gap between the QMF prediction and the simulated threshold when  $\gamma > 3$ . Since the disassortative degree-degree correlations exist when  $\gamma < 3$ , there is a slight difference between  $\lambda_c^{HMF}$  and  $\lambda_p^\Delta$ . Specially, Fig. 4 (d) shows a more clear distinction between  $\lambda_c^{HMF}$  and  $\lambda_p^\Delta$  for SFNs with natural cutoff when  $\gamma = 2.25$ , while the QMF prediction is very close to the simulated threshold for the principle eigenvector is delocalized when  $2 < \gamma \leq 5/2$  [39]. From above analysis, we can conclude that, in most cases, the HMF theory is more accurate than the QMF theory for predicting the SIR threshold on SFNs.

### B. Epidemic threshold of real networks

To further check the performances of the susceptibility  $\chi$  and variability  $\Delta$ , Fig. 5 depicts  $\chi$  and  $\Delta$  on Hamsterster full (containing friendships and family links between users of the website hamsterster.com) and Facebook (NIPS) (containing Facebook user-user friendships) networks. The simulated results intuitively show that the variability  $\Delta$  always reaches a maximum near the critical point of  $\rho$  (i.e.,  $\lambda_c$ ) for both SIS and SIR models. However, the peak of the susceptibility  $\chi$  appears at a larger  $\lambda$  in the SIR model, which is similar to the results in Sec. II. The theoretical predictions of the HMF theory and of the QMF theory are quite close to the numerical threshold determined by  $\Delta$  on Hamsterster full network, which is assortative, but they become poor on Facebook (NIPS) network, which is disassortative.

More detailed comparisons between the simulated and theoretical thresholds on real networks are presented in Table I. For the SIR model, the simulated threshold determined by the susceptibility (i.e.,  $\lambda_p^\chi(SIR)$ ) is larger than that obtained by the variability measure (i.e.,  $\lambda_p^\Delta(SIR)$ ). Although the HMF prediction and the simulated threshold  $\lambda_p^\Delta(SIR)$  are nearly the same for assortative networks, there is an obvious difference between them for networks showing significant disassortative mixing. The QMF prediction is relatively worse than the HMF prediction for assortative networks, but the former

is close to  $\lambda_p^\Delta(SIR)$  for some disassortative networks (e.g., Router views, CAIDI, and email contacts). The two simulated thresholds of the SIS model, i.e.,  $\lambda_p^\chi(SIS)$  and  $\lambda_p^\Delta(SIS)$ , are nearly the same in most of real networks. By calculating the inverse participation ratio  $IPR(\Lambda)$  of real networks [39], we find that, the QMF prediction agrees well with the simulated thresholds of the SIS model when  $IPR(\Lambda) \rightarrow 0$  [i.e., the principal eigenvector of the adjacency matrix of a network  $f(\Lambda)$  is delocalized], but becomes poor when  $IPR(\Lambda)$  is large [i.e., the eigenvector  $f(\Lambda)$  is localized]. This result agrees with the conclusion of Ref. [39] to a certain extent.

## V. CONCLUSIONS

In summary, we have studied the simulated identification of epidemic threshold on complex networks with finite size. First, the accuracies of the susceptibility and variability measures are checked by applying them on RRNs, in which the HMF is exact. We have shown that the variability  $\Delta$  is valid for determining the simulated thresholds of the SIS and SIR models, while the susceptibility  $\chi$  gives a larger SIR threshold.

In order to get a deep understanding of the two estimation methods, we have analyzed the epidemic spreading near the critical point  $\lambda_c$ . For the SIS model, the epidemic quickly dies out when  $\lambda < \lambda_c$ . When  $\lambda \simeq \lambda_c$ , although the prevalence approximates an exponential distribution, the probability of  $\rho = 0$  is still maximum. Above the threshold  $\lambda > \lambda_c$ , the prevalence is distributed homogeneously. For the SIR model, the outbreak sizes follow approximately an exponential distribution when  $\lambda < \lambda_c$ . At the critical point, the outbreak sizes follow a power-law distribution with the exponent -1.5. When  $\lambda \rightarrow \lambda_c^+$ , the simulated distribution of outbreak sizes is bimodal with two peaks occurring at  $\rho = 1/N$  and  $O(1)$ . The probability of small outbreak size in theory is consistent with that obtained by numerical simulations, but the probability of large outbreak sizes that constitute a lump in the simulated scattergram can not be obtained theoretically. Based on reasonable cutoff hypothesis, we find the susceptibility measure can give a quite accurate SIR threshold when the second lump is ignored. Since the variability measure reflects the relative fluctuation of epidemic spreading, it is always effective in determining the epidemic threshold, where the distribution of outbreak sizes has a very strong heterogeneity.

Moreover, the simulated thresholds of the SIR model are investigated on scale-free and real networks. All results indicate that the epidemic threshold determined by the variability  $\Delta$  is more accurate than that from the susceptibility  $\chi$ . The HMF prediction is in general more accurate, but it becomes worse due to the existence of disassortative mixing on SFNs with natural cutoff and  $\gamma < 5/2$ . Similarly, the HMF approximation is accurate for the SIR model on real networks with assortative mixing, while it becomes very poor on disassortative networks. We further confirm that the QMF prediction, which is not accurate enough on assortative network, is valid on some disassortative networks.

We here put forward an estimation method, whose effec-

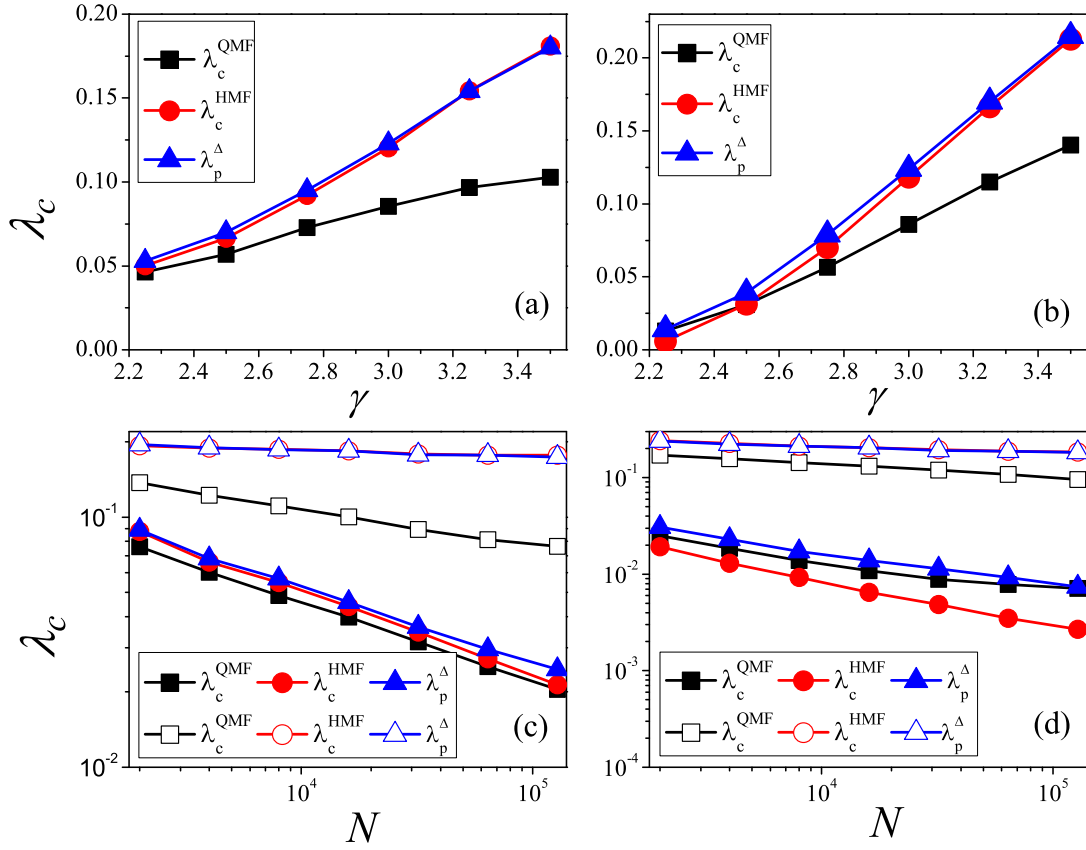


FIG. 4: (Color online) Comparison of theoretical thresholds with simulated thresholds on SFNs.  $\lambda_c$  vs.  $\gamma$  for SFNs with structural cutoff (i.e.,  $k_{\max} \sim N^{1/2}$ ) (a) and nature cutoff (i.e.,  $k_{\max} \sim N^{\frac{1}{\gamma-1}}$ ) (b), where  $N$  is set at  $10^4$ .  $\lambda_c$  vs.  $N$  for SFNs with structural cutoff (c) and nature cutoff (d), where solid and empty symbols denote  $\gamma = 2.25$  and  $3.50$ , respectively. “squares”, “circles” and “triangles” denote  $\lambda_c^{\text{QMF}}$ ,  $\lambda_c^{\text{HMF}}$  and  $\lambda_p^{\Delta}$ , respectively.

TABLE I: Topology characteristics and epidemic thresholds of real networks.  $N$  is the network size,  $k_{\max}$  is the maximum degree,  $r$  is the degree correlations,  $\lambda_c^{\text{HMF}}(\text{SIS})$  is the HMF prediction of SIS threshold,  $\lambda_c^{\text{HMF}}(\text{SIR})$  is the HMF prediction of SIR threshold, and  $\Lambda_N$  is the largest eigenvalue of adjacent matrix.

Network	$N$	$k_{\max}$	$r$	$\lambda_c^{\text{HMF}}(\text{SIS})$	$\lambda_c^{\text{HMF}}(\text{SIR})$	$\lambda_c^{\text{QMF}}$	$\lambda_p^{\Delta}(\text{SIR})$	$\lambda_p^{\chi}(\text{SIR})$	$\lambda_p^{\Delta}(\text{SIS})$	$\lambda_p^{\chi}(\text{SIS})$	$\text{IPR}(\Lambda_N)$
Hamsterster full [40]	2000	273	0.023	0.023	0.023	0.020	0.023	0.108	0.025	0.025	0.009
Brightkite [40]	56739	1134	0.010	0.016	0.016	0.010	0.014	0.238	0.012	0.012	0.006
arXiv astroPh [40]	17903	504	0.201	0.015	0.015	0.011	0.012	0.09	0.012	0.012	0.004
Pretty Good Privacy [41]	10680	206	0.239	0.053	0.056	0.024	0.053	0.477	0.033	0.033	0.017
US power grid [42]	4941	19	0.003	0.258	0.348	0.134	0.446	0.496	0.261	0.264	0.041
Euroroad [43]	1039	10	0.090	0.324	0.479	0.249	0.498	0.711	0.331	0.331	0.049
Facebook(NIPS) [40]	2888	769	-0.668	0.004	0.004	0.036	0.075	0.494	0.079	0.497	0.244
Route views [40]	6474	1458	-0.182	0.006	0.006	0.022	0.037	0.345	0.034	0.496	0.087
CAIDA [40]	26475	2628	-0.195	0.004	0.004	0.014	0.019	0.336	0.019	0.019	0.024
email contacts [44]	12625	576	-0.387	0.009	0.009	0.02	0.027	0.404	0.024	0.025	0.013

tiveness has been verified by analyzing the critical distribution. This method can be applied to the precise determination of epidemic threshold on various networks, and could be extended to other dynamic processes such as information diffusion and behavior spreading. Besides, the accurate analytic approximation of the epidemic threshold for general networks remains an important problem. This work helps to

verify theoretical analysis of critical point and would promote further study on phase transition of epidemic dynamics.

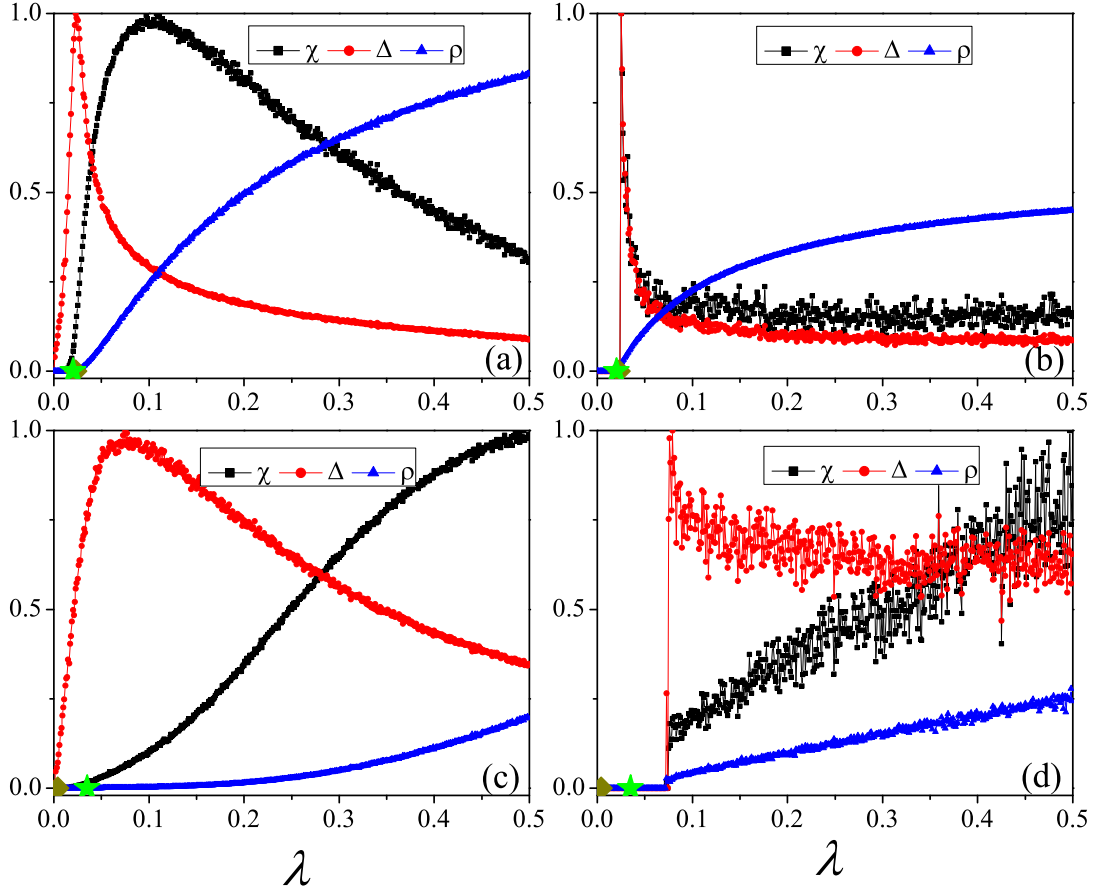


FIG. 5: (Color online) Susceptibility  $\chi$  and variability  $\Delta$  as a function of  $\lambda$  on real networks.  $\chi$ ,  $\Delta$  and  $\rho$  vs.  $\lambda$  for SIR (a) and SIS (b) on Hamsterster full network.  $\chi$ ,  $\Delta$  and  $\rho$  vs.  $\lambda$  for SIR (c) and SIS (d) on Facebook (NIPS) network. “squares”, “circles” and “triangles” denote  $\chi$ ,  $\Delta$  and  $\rho$ , respectively. “green star” denotes  $\lambda_c^{\text{QMF}} = 1/\Lambda_N$ , “yellow diamond” denotes  $\lambda_c^{\text{HMF}} = \langle k \rangle / [\langle k^2 \rangle - \langle k \rangle]$  in (a) and (c), and  $\lambda_c^{\text{HMF}} = \langle k \rangle / \langle k^2 \rangle$  in (b) and (d). The susceptibility  $\chi$  and variability  $\Delta$  are normalized with  $\chi_{\max}$  and  $\Delta_{\max}$ , respectively.

#### ACKNOWLEDGEMENTS

This work was partially supported by National Natural Science Foundation of China (Grant Nos. 11105025, 91324002), China Postdoctoral Science Special Foundation (Grant No. 2012T50711), the Program of Outstanding Ph. D. Candidate in Academic Research by UESTC (Grand No. YXB-SZC20131033) and Open Foundation of State key Laboratory of Networking and Switching Technology (Beijing University of Posts and Telecommunications) (SKLNST-2013-1-18).

#### APPENDIX: THE THEORETICAL DISTRIBUTION OF SMALL OUTBREAK SIZES

For the case of the SIR model and similar models with no steady-state, the static properties (e.g., the final outbreak size and the critical point) of the epidemic outbreak can be mapped into a suitable bond percolation problem. In this framework, the distribution of occupied cluster sizes is related to the distribution of outbreak sizes. To get the distribution of small out-

break size in the SIR model with  $\lambda$  and recovery rate  $\mu = 1$ , we will present the derivation of the distribution of small occupied cluster sizes in bond percolation with bond occupation probability  $\lambda$  [19].

After the percolation process on a general network with arbitrary degree distribution  $p_k$ , the average degree of the occupied network  $A_1$ , which composes of vertices and occupied edges, is  $\langle k_T \rangle = \lambda \langle k \rangle$ , where  $\langle k \rangle$  is the average degree of the original network  $A_0$ . And the distribution of the small subgraphs of network  $A_1$  is

$$\pi_s = \frac{\langle k_T \rangle}{(s-1)!} \left[ \frac{d^{s-2}}{dz^{s-2}} [g_1(z)]^s \right]_{z=0}, \quad (7)$$

where  $g_1(z)$  is the generating function of the excess degree of network  $A_1$ . In addition, the generating function of degree distribution of  $A_1$  is

$$g_0(z) = \sum_{k=0}^{\infty} p_k (1 - \lambda + z\lambda)^k,$$

and

$$g_1(z) = \frac{g'_0(z)}{g'_0(1)}$$

Thus, in a random regular network, which has a unique degree  $k$  with  $p_k = 1$ , we can easily obtain that

$$g_0(z) = [1 + (z - 1)\lambda]^k, \quad (8)$$

and

$$g_1(z) = [1 + (z - 1)\lambda]^{k-1}. \quad (9)$$

Substituting Eq. (9) into Eq. (7), we can obtain the distribution of small outbreak sizes of the disease as follow:

$$\pi_s = \frac{k\Gamma(a_2)}{\Gamma(a_0)\Gamma(a_1)} \lambda^{s-1} (1 - \lambda)^{s(k-1)-(s-2)}, \quad (10)$$

where  $\Gamma(x+1) = x!$ ,  $a_0 = (s-2)$ ,  $a_1 = s(k-1) - (s-1)$ , and  $a_2 = s(k-1) - 1$ .

- 
- [1] A. Barrat, M. Barthélemy, and A. Vespignani, *Dynamical Processes on Complex Networks* (Cambridge University Press, Cambridge, England, 2008).
  - [2] A. Vespignani, *Nat. Phys.* **8**, 32 (2012).
  - [3] R. M. Anderson and R. M. May, *Infectious Diseases in Humans* (Oxford University, Oxford, 1992).
  - [4] R. Pastor-Satorras, C. Castellano, P. V. Mieghem, and A. Vespignani, arXiv:1408.2701.
  - [5] S. N. Dorogovtsev, A. V. Goltsev, and J. F. F. Mendes, *Rev. Mod. Phys.* **80**, 1275 (2008).
  - [6] R. Pastor-Satorras and A. Vespignani, *Phys. Rev. E* **63**, 066117 (2001).
  - [7] R. Pastor-Satorras and A. Vespignani, *Phys. Rev. Lett.* **86**, 3200 (2001).
  - [8] M. Boguñá, and R. Pastor-Satorras, *Phys. Rev. E* **66**, 047104 (2002).
  - [9] M. E. J. Newman, *Networks: An Introduction* (Oxford University Press, Oxford, England, 2010).
  - [10] R. Albert and A. -L. Barabási, *Rev. Mod. Phys.* **74**, 47 (2002).
  - [11] M. E. J. Newman, *Contemp. Phys.* **46**, 5 (2005).
  - [12] O. Givan, N. Schwartz, A. Cygelberg, and L. Stone, *J. Theor. Biol.* **288**, 21 (2011).
  - [13] D. Chakrabarti, Y. Wang, C. Wang, J. Leskovec, and C. Faloutsos, *ACM Trans. Inf. Syst. Secur.* **10**, 1 (2008).
  - [14] P. Van Mieghem, J. Omic, and R. Kooij, *IEEE ACM Trans. Netw.* **17**, 1 (2009).
  - [15] S. Gómez, A. Arenas, J. Borge-Holthoefer, S. Meloni, and Y. Moreno, *Europhys. Lett.* **89**, 38009 (2010).
  - [16] F. Chung, L. Lu, and V. Vu, *Proc. Natl. Acad. Sci. USA* **100**, 6313 (2003).
  - [17] E. Cator and P. Van Mieghem, *Phys. Rev. E* **85**, 056111 (2012).
  - [18] M. Barthélemy, A. Barrat, R. Pastor-Satorras, and A. Vespignani, *Phys. Rev. Lett.* **86**, 3200 (2004).
  - [19] M. E. J. Newman, *Phys. Rev. E* **66**, 016128 (2002).
  - [20] J. P. Gleeson, *Phys. Rev. Lett.* **107**, 068701 (2011).
  - [21] J. Marro and R. Dickman, *Nonequilibrium Phase Transitions in Lattice Models* (Cambridge University Press, Cambridge, England, 1999).
  - [22] K. Binder and D. W. Heermann, *Monte Carlo Simulation in Statistical Physics*, 5th ed. (Springer-Verlag, Berlin, 2010).
  - [23] M. Boguñá, C. Castellano and R. Pastor-Satorras, *Phys. Rev. Lett.* **111**, 068701 (2013).
  - [24] S. C. Ferreira, R. S. Ferreira, C. Castellano, and R. Pastor-Satorras, *Phys. Rev. E* **84**, 066102 (2011).
  - [25] H. Hong, M. Ha, and H. Park, *Phys. Rev. Lett.* **98**, 258701 (2007).
  - [26] S. C. Ferreira, C. Castellano, and R. Pastor-Satorras, *Phys. Rev. E* **86**, 041125 (2012).
  - [27] C. Castellano and R. Pastor-Satorras, *Sci. Rep.* **2**, 371 (2012).
  - [28] C. Castellano and R. Pastor-Satorras, *Phys. Rev. Lett.* **105**, 218701 (2010).
  - [29] P. Crépey, F. P. Alvarez, and M. Barthélemy, *Phys. Rev. E* **73**, 046131 (2006).
  - [30] P. Shu, M. Tang, K. Gong, and Y. Liu, *Chaos* **22**, 043124 (2012).
  - [31] A. S. Mata, R. S. Ferreira, and S. C. Ferreria, *New J. Phys.* **16**, 053006 (2014).
  - [32] E. Ben-Naim and P. L. Krapivsky, *Phys. Rev. E* **69**, 050901(R) (2004).
  - [33] E. Ben-Naim and P. L. Krapivsky, *Eur. Phys. J. B* **85**, 1 (2012).
  - [34] D. A. Kessler and N. M. Shnerb, *Phys. Rev. E* **76**, 010901(R) (2007).
  - [35] D.H. Zanette, *Phys. Rev. E* **64**, 050901(R) (2001).
  - [36] A. Khalleque and P. Sen, *J. Phys. A: Math. Theor.* **46**, 095007 (2013).
  - [37] M. Boguñá, R. Pastor-Satorras, and A. Vespignani, *Eur. Phys. J. B* **38**, 205 (2004).
  - [38] H. K. Lee, P.-S. Shim, and J.D. Noh, *Phys. Rev. E* **87**, 062812 (2013).
  - [39] A. V. Goltsev, S. N. Dorogovtsev, J. G. Oliveira, and J. F. F. Mendes, *Phys. Rev. Lett.* **109**, 128702 (2012).
  - [40] See <http://konect.uni-koblenz.de/networks/>.
  - [41] M. Boguñá, R. Pastor-Satorras, A. Diaz-Guilera, and A. Arenas, *Phys. Rev. E* **70**, 056122 (2004).
  - [42] D. J. Watts and S. H. Strogatz, *Nature* **393**, 440 (1998).
  - [43] L. Šubelj and M. Bajec, *Eur. Phys. J. B* **81**, 353 (2011).
  - [44] M. Kitsak, L. Gallos, S. Havlin, F. Liljeros, L. Muchnik, H. Stanley, and H. Makse, *Nat. Phys.* **6**, 888 (2010).